Proton Antenna Effect of the γ-Cyclodextrin Outer Surface, Measured by Excited State Proton Transfer

Rinat Gepshtein,[†,‡] Pavel Leiderman,[†] Dan Huppert,[*,†] Elad Project,[§,‡] Esther Nachliel,[§] and Menachem Gutman[§]

Raymond and Beverly Sackler Faculty of Exact Sciences, School of Chemistry, Tel Aviv University, Tel Aviv 69978, Israel, and Laser Laboratory for Fast Reactions, Biochemistry, Tel Aviv University, Tel Aviv 69978, Israel

Received: August 9, 2006; In Final Form: September 21, 2006

The reversible proton dissociation and geminate recombination of the common photoacid, 8-hydroxypyrene-1,3,6-trisulfonate (pyranine), either in dilute aqueous solution or when forming a complex with γ-cyclodextrin (γ-CD), has been studied by time-resolved fluorescence spectroscopy and supplemented by molecular modeling and dynamics simulations. We find that the dissociation rate of the proton from the excited molecule was decreased to about ∼50% of its value in water, while the rate of recombination was doubled. These observations were evaluated by molecular modeling of the reactants at atomic resolution. The combination of the two methodologies indicates that the pyranine in the complex can assume more than one level of interaction with the solvent. The polysugar torus surrounding the pyranine perturbs the hydrogen bond in the dye's immediate vicinity and deforms the electrostatic potential inside the Coulomb cage, causing major deviations from a simple spheric symmetry. These observations can account for the special kinetic features measured for the complex. We suggest that this system can be used as a basic model for evaluating the mechanism of proton transfer in non-homogeneous systems, such as the surface of proteins or biomembranes.

Introduction

Proton transfer reactions are common in chemical and biological processes.[1−4] Over the last two decades, intermolecular proton transfer in the excited state (ESPT) has been studied extensively and provided pertinent information about the mechanism and the parameters controlling acid−base reactions.[5−12]

To initiate these reactions, protic solvent solutions of photoacids are irradiated by short (femtosecond−picosecond) laser pulses.[13,14] Consequently, the excited state molecules dissociate very rapidly by transfer of a proton to a nearby solvent molecule. 8-Hydroxypyrene-1,3,6-trisulfonate (HPTS or pyranine) is a photoacid commonly used in the study of the ESPT process.[15,16] The RO^- form is a quadrupled charged body ($Z = -4$), rendering the reversible geminate recombination process to be much enhanced relative to that of a single charged photoacid like 2-naphthol. The proton transfer rate could be determined either by the initial decay time of the time-resolved fluorescence of the protonated form (ROH*) measured at 440 nm or by the slow rise time of the emission of the deprotonated species (RO^-) at about 520 nm. The simple spheric symmetry of the back reaction, where the anion is represented by a Coulomb cage that reacts with external reactants (free proton or proton scavengers) while the propagation of the proton inside the Coulomb cage is given by the Debye−Smoluchowski equations, strongly facilitated the analysis of the process, as embedded in the geminate recombination formalism.

The ease of study of the dynamics of the reversible proton transfer was exploited for investigating the properties of local environment. Photoacids were used in confined nanometric volumes such as proteins,[17−19] liposomes,[20] and reverse micelles,[21] and the effects of the confining boundary surrounding the photoacid molecule were derived by the geminate recombination analysis. While in the above studies the photoacid was totally "immersed" in a homogeneous matrix, the binding by cyclodextrins generates another situation, where the photoacid is inserted in a nonpolar ring while it is still exposed to the bulk water.

Cyclodextrins are water-soluble inclusion complexes containing a hydrophobic cavity that binds apolar molecules of a size smaller than its cavity diameter to form a host−guest inclusion complex. γ-Cyclodextrin (γ-CD) is composed of a cyclic oligomer containing eight glucose units. The height of the γ-CD cavity is about 8 Å, and the maximum inner diameter is 9.5 Å. The two rims of the torroid structure contain many OH groups (primary and secondary hydroxyl rims). Each glucose unit contributes two secondary OH groups to one rim, which will be referred to as the 16OH rim. The opposite rim (the 8OH rim) of γ-CD contains $-CH_2OH$ groups, one from each glucose unit, altogether eight CH_2OH groups. Those OH groups serve according to our model as proton collectors and are capable of transporting effectively a proton along the hydroxylic rim of the cyclodextrin. Gill and co-workers[22] studied several photoacids in the presence of α- and β-cyclodextrin. Inclusion complexes of 1,6-naphthalenediol (ND) inside the CD cavity blocked proton transfer in photoexcited ND.[22] The photoprotolytic reaction of 1-naphthol and several other photoacids in the β-cyclodextrin inclusion complex was comprehensively studied by Kozwmenko et al.[23−25] Excited state proton transfer in inclusion complexes of 1-aminopyrene and α-naphthol with

* Corresponding author. E-mail: huppert@tulip.tau.ac.il. Phone: 972-3-6407012. Fax: 972-3-6409293.
[†] Raymond and Beverly Sackler Faculty of Exact Sciences.
[‡] These authors made an equal contribution to this study.
[§] Laser Laboratory for Fast Reactions.

10.1021/jp065139w CCC: $33.50
Published on Web 11/23/2006

cyclodextrins was studied by Hansen et al.[26] using time-resolved emission spectroscopy. The data suggested two distinct binding orientations for 1-aminopyrene bound to β-CD. The rate of proton transfer is increased by a factor of 2−3 compared to pure water**.** On the other hand, in the case of α-naphthol, the rate of proton transfer slows down considerably in the inclusion complex. The diversity of the kinetic effect and acceleration or slowing down of the initial proton dissociation indicate that the local conditions within the CD structure are diverse, reflecting a very non-homogeneous space. Recently, Bahattacharyya and co-workers[27] focused their attention on the ESPT process of pyranine in the nanocavity of a large cyclodextrin compound, the γ-CD. They found that the ESPT of pyranine is slowed inside γ-CD as compared to bulk water. They also found that recombination of the geminate ion pair in the inclusion complex is 3.5 faster than it is in water. To explain these effects, it was assumed that the proton transfer process is locally confined by the γ-CD interior structure. Since the inside space of the cyclodextrin cavity is small, there is a very limited probability for proton diffusion enhancing the recombination reaction.

In the present study, we report on excited state proton transfer and geminate recombination measurements with the pyranine−γ-CD inclusion complex in neat water or in the presence of other solutes. Besides the kinetic analysis, we introduced in this study molecular dynamics simulations of the reactants, in an attempt to obtain a visual imaging of the reaction space. The combination of the two methodologies provides an explanation as to some peculiarities of the rate constants which were not fully consistent with a simple spheric symmetry of the reaction space. Unlike proton transfer in bulk water, where the reaction sphere surrounding the pyranine can be approximated as a set of concentric shells, the insertion of the pyranine inside the γ-CD torroid structure alters the inner "anatomy" of the Coulomb cage. The nonspheric boundary, caused by the low dielectric constant matrix, together with the specific interactions between the hydroxyl residues of the sugar structures with the water, complicates the passage of a proton within the immediate vicinity of the pyranine−γ-CD inclusion complex process. These peculiarities can be explained by referring to the precise shape of the reaction sphere, and the local electrostatic potentials, as derived by molecular modeling. The mechanism of proton transfer within a non-homogeneous electrostatic field is discussed.

Materials and Methods

Time-resolved fluorescence was acquired by use of the time-correlated single-photon counting (TCSPC) technique, the method of choice when sensitivity, a large dynamic range, and low intensity illumination are important criteria in fluorescence decay measurements.

For excitation, we used a cavity-dumped Ti:sapphire femtosecond laser, Mira Coherent, which provides short, 80 fs pulses of variable repetition rate, operating at the second-harmonic generation (SHG) frequency, over the spectral range 380−400 nm with a relatively low repetition rate of 500 kHz. The TCSPC detection system is based on a Hamamatsu 3809U photomultiplier and Edinburgh Instruments TCC 900 computer module for TCSPC. The overall instrumental response was about 35 ps (fwhm). Measurements were taken at a spectral width of 10 nm. The excitation pulse energy was reduced by neutral density filters to about 10 pJ. We checked the sample's absorption prior to and after time-resolved measurements. We could not find noticeable changes in the absorption spectra due to sample irradiation.

Steady state fluorescence spectra were taken using a FluoroMax (Jobin Yvon) spectrofluorometer. The HPTS, of laser grade, was purchased from Kodak or Aldrich. Perchloric acid, 70% reagent grade, was purchased from Aldrich. γ-CD 99% was purchased from Acros Organics.

The concentrations of HPTS complexed with the γ-CD were between 2×10^{-6} and 2×10^{-5} M. The γ-CD concentration was 30 mM. Deionized water had a resistance of >10 MΩ. γ-CD hydrate (99%) was purchased from Acros Organics. All chemicals were used without further purification. The solution pH was about 6.

The HPTS fluorescence spectrum consists of two structureless broad bands (∼40 nm fwhm). The emission band maxima of the acidic form (ROH*) and the alkaline form (RO^-*) in water are at 435 and 510 nm, respectively. At 435 nm, the overlap of the two luminescence bands is rather small. The contribution of the RO^-* band to the total intensity at 435 nm is less than 0.2%. To avoid overlap between contributions of the two species, we mainly monitored the ROH* fluorescence at 435 nm.

Reversible Diffusion-Influenced Two-Step Proton Transfer and Geminate Recombination (GR) Model. In this model,[12,15,16] the overall dissociation process can be subdivided into the two consecutive steps of reaction and diffusion. In the reactive stage, a rapid short-range charge separation occurs and a solvent-stabilized ion pair is formed. This is followed by a diffusive stage, when the two ions withdraw from each other due to their thermal random motion. The reverse process is a geminate recombination (neutralization) of the two separated ions, either by the direct collapse of the ion pair or following a geminate re-encounter of the solvated "free" ions.

The mathematical and computational details are given elsewhere.[16,28] It is based on solving the Debye Smoluchowski equation (DSE), coupled to an ordinary chemical kinetic equation. As compared with traditional treatments of diffusion-influenced reactions,[29] the new aspect is the reversibility of the reaction, described by the "backreaction" boundary conditions.[16,30,31]

The proton bound (ROH) and dissociated (RO^-) states evolve according to the DSE. We solve the equations numerically using the Windows application[32] for solving the spherically symmetric diffusion problem (SSDP); we convolute the solution with the instrument response function (IRF) of the time-correlating single-photon counting system and compare it to the ROH* fluorescence signal. The asymptotic expression (the long-time behavior) for the fluorescence of ROH* in the case where both forms of the photoacid, ROH* and RO^-*, have the same lifetime is given by eq 1.[31]

$$[\mathrm{ROH}^*]\exp[t/\tau_f] \cong \frac{\pi}{2}a^2(\exp[V(a)])\frac{k_r}{k_{PT}(\pi D)^{3/2}}t^{-d/2} \quad (1)$$

where τ_f is the excited state lifetime of both the protonated form, ROH*, and the deprotonated form, RO^-, d is the dimensionality of the relevant problem, a is the contact radius, k_{PT} and k_r are the proton transfer and recombination rate constants, respectively, D is the mutual diffusion constant of RO^-* and H^+, and $V(a)$ is the Coulomb potential at the contact distance a. Equation 1 shows that the tail amplitude depends on several parameters, but its time dependence is a power law of time that depends on the dimensionality of the problem. For three dimensions, it assumes the power law of $t^{-3/2}$.

k_{PT} determines the initial slope of the decay curves: the larger k_{PT}, the faster the initial exponential drop. The intrinsic

recombination rate constant, k_r, has no effect on the behavior at $t \rightarrow 0$ but determines the magnitude of the long-time tail. The effect of an increase of k_r is somewhat similar to a decrease of D. It differs from the effect of changing R_D or a in the curvature of these plots. The parameters for the numerical solution of the DSE were taken from the literature.[33] The contact radius in aqueous solution, $a = 6$ Å, is slightly larger than the molecule's spherical gyration radius (4.5−5.5 Å), obtained from measurements of HPTS rotation times.[34] It probably accounts for at least one layer of water molecules around the HPTS anion. In the data fitting of HPTS in γ-CD, we used a contact radius of ∼4.5 Å. We found that the quality of the fit with a larger contact radius is rather poor.

Molecular Dynamics Simulation of Pyranine and Pyranine−γ-Cyclodextrin. The molecular dynamics (MD) simulations were performed using the GROMACS 3.2.1 package of programs[35−37] with the GROMOS96 force field.[38] The starting structure of γ-cyclodextrin was obtained from ref 39. The starting structure of pyranine and the MD parametrization of both molecules were obtained from the PRODRG server for small molecules.[40] In the pyranine−γ-cyclodextrin simulation, the pyranine was "manually" inserted into the γ-cyclodextrin belt torus using VMD.[41] In the pyranine and pyranine−γ-cyclodextrin simulations, the molecules were embedded in a box containing the SPC water model[42] that extended to at least 15 Å between the molecules and the edge of the box. In the γ-cyclodextrin, the distance was 12 Å. The numbers of water molecules were 1638, 1752, and 2736 for the pyranine, γ-cyclodextrin, and pyranine−γ-cyclodextrin simulations, respectively. To neutralize the system and to reach a physiological ionic strength of 200 mM, five sodium and two chloride ions were added for the pyranine simulation, four sodium and four chloride ions were added for the γ-cyclodextrin simulation, and seven sodium and four chloride ions were added for the pyranine−γ-cyclodextrin simulation, in random positions. Prior to the dynamics simulation, internal constraints were relaxed by energy minimization. Following the minimization, a MD equilibration run was performed under position restraints for 50 ps. After the equilibration, a MD production run was performed for a duration of 6.2 ns for the pyranine−γ-cyclodextrin and γ-cyclodextrin simulations and 4.2 ns for the pyranine simulation. During the MD run, the LINCS algorithm[43] was used in order to constrain the lengths of all bonds; the waters were restrained using the SETTLE algorithm.[44] The time step for the simulation was 2 fs. The simulations were run under NPT conditions, using Berendsen's coupling algorithm to keep the temperature and the pressure constant ($P = 1$ bar; $\tau_P = 0.5$ ps; $T = 300$ K; $\tau_T = 0.1$ ps).[45] van der Waals (VDW) forces were treated using a cutoff of 12 Å. Long-range electrostatic forces were treated using the particle mesh Ewald (PME) method.[46]

The criteria taken for H-bonds are the default set in the GROMACS utility g_hbond: a 30° cutoff for the donor−acceptor−hydrogen angle and a 0.35 nm cutoff distance between the acceptor and the donor. OH and NH are donors, and O and N are acceptors.

The coordinates were saved every 1 ps. All figures were created using the VMD computer program.[41]

Electrostatic Potential Calculations for the Pyranine and Pyranine−γ-Cyclodextrin. The electrostatic potentials around the pyranine and pyranine−γ-cyclodextrin were calculated by solvation of the nonlinear Poisson−Boltzmann (PB) equation. The pyranine anion and the pyranine anion in the γ-cyclodextrin ring were first geometry optimized using the computer program GAMESS,[47] and RHF with the AM1 basis set. After optimization, the atomic charges were calculated using the RHF and N31 basis set. The atomic radii were taken from Gromacs. The solvent was represented as a continuum with a dielectric constant of $\epsilon = 78.54$. The dielectric constant of the solute was defined as $\epsilon = 2$. The nonlinear PB equation was solved by the computer program APBS[48] using a grid with a spacing of $0.465 \times 0.465 \times 0.465$ and $1.83 \times 0.465 \times 0.465$ Å^3 for the pyranine and pyranine−γ-cyclodextrin, respectively, with an ionic strength of 70 mM, 100 mM, and 120 μM. The potentials were presented using the computer program VMD.[41]

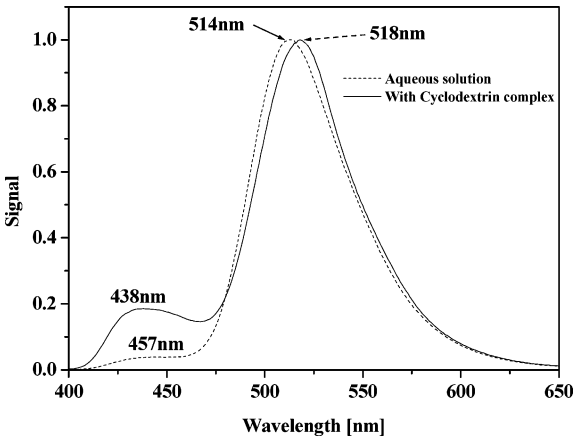

Figure 1. Steady state emission (solid line) of HPTS in the inclusion complex with γ-CD excited at the ROH* absorption band at 395 nm. As a comparison, the steady state emission of HPTS in water is also shown (dashed line). The γ-CD concentration was about 30 mM, while that of HPTS was 4×10^{-6} M.

Results

Steady State Emission. The steady state emission of HPTS was measured for the pyranine either in water (Figure 1, solid line) or for the inclusion complex with γ-CD (dotted line). Both spectra are normalized with respect to the maximal emission of RO^-*. The excitation was at the maximum of the ROH absorption band ($\lambda = 395$ nm). To ensure that all of the pyranine is in the γ-CD complex form, the γ-CD concentration was set to 30 mM, while that of HPTS was 4×10^{-6} M. At this ratio, the free form of the pyranine is negligible.

Examination of the emission spectrum reveals a 5-fold amplification of the complex ROH* emission with respect to that of the free photoacid. The position of the ROH* emission band in the inclusion complex is blue-shifted with respect to the band in solution and is more structured. In parallel, there is a distinct red shift of the RO^-* emission with respect to that of the free form, 518 nm versus 514 nm in aqueous solution. These results are accountable by our previous studies of the solvatochromic shift of photoacid as measured in various solvents.[49−51] For the ROH* emission band, the blue shift indicates a decrease of the solvent polarity and of the hydrogen bonding accepting power (with respect to water) of the solvent. The red shift of RO^-* implies that the water molecules in the immediate vicinity of the excited pyranine are a poorer hydrogen-bond donor. Thus, in the inclusion complex, the average solvent properties such as polarity and hydrogen bond donating and accepting powers that the HPTS experiences are slightly smaller than those in bulk water but still much larger than those in an apolar aprotic solvent. This observation implies that γ-CD affects the properties of the water molecules with which the dye is interacting.

Time-Resolved Emission. The fluorescence decay curves of pyranine, either as a free pyranine or when inserted in the torus

TABLE 1: Kinetic Parameters for the Proton Transfer Reaction of HPTS in Bulk Water and γ-CD

	k_{PT}[a] (10^9 s^{-1})	k_r[a,b] (10^9 Å·s^{-1})	R_D (Å)	D_{H^+} (cm^2 s^{-1})	τ_{ROH} (ns)	τ_{RO^-} (ns)	k_{sc}[c] (s^{-1})
H_2O	9.5	9	28.2	1×10^{-4}	5.4	5.4	
D_2O	3.9 (2.4)	3*(3.3)	28.2	0.67×10^{-4}	9.2	12.5	
γ-CD/H_2O	4.5	18	28.3	1×10^{-4}	5.3	5.9	8.5×10^7
γ-CD/D_2O	2.2 (2.2)	11.5 (1.6)	28	0.67×10^{-4}	9.2	12.5	$>1 \times 10^7$

[a] k_{PT} and k_r are obtained from the fit of the experimental data by the reversible proton transfer model (see text). [b] The error in the determination of k_r is 50%; see text. [c] k_{sc}, pseudo-first-order proton scavenging rate constant; see text.

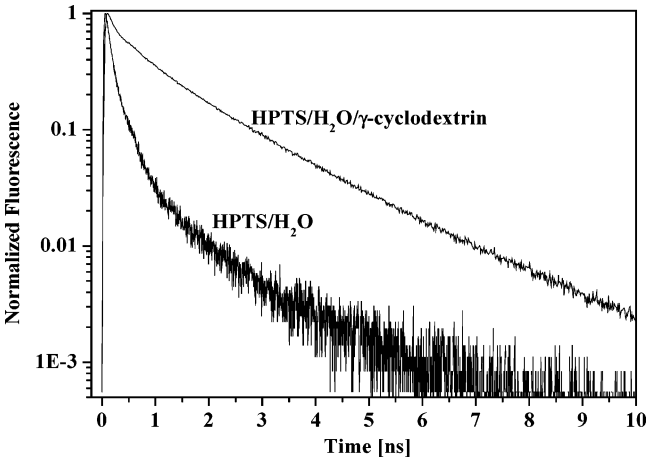

Figure 2. Time-resolved emission of the ROH* band of HPTS in bulk water and in the inclusion complex.

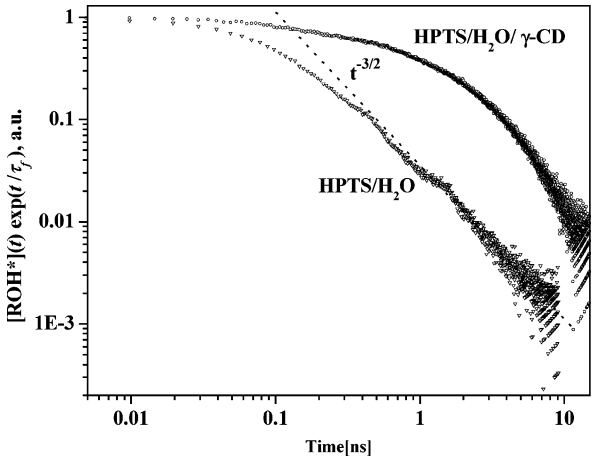

Figure 3. Log−log plot of the ROH × exp(t/τ) decay of pyranine in aqueous solution and in the inclusion complex with γ-CD. While the data for pyranine in bulk water follow a power law of $t^{-3/2}$, the cyclodextrin complex data deviate from the power law.

of γ-CD ($I \leq 100$ μM) are presented in Figure 2. The sample was excited by a 400 nm femtosecond pulse at a repetition rate of 500 kHz, and the emission was measured at 435 nm. The difference between the signals is apparent. In water, the ROH* emission decays rapidly, and at the first 200 ps, about 90% of the signal's intensity had vanished in a practically first-order reaction. When locked in the γ-CD, the relaxation of the ROH* emission is significantly slower. During the first ~200 ps, the reaction is somewhat faster than the rest of the relaxation and the amplitude of this phase is not more than ~30% of the signal intensity.

The kinetic analysis of the signals is based on the geminate recombination formalism, which assumes that the reaction space is a set of concentric spheric shells with the RO^-* located in the center. The proton propagates in the radial direction, while any normal motion is considered as a delay in the radial motion. The formalism defines a transition probability between concentric rings as a function of the gradient of the electrostatic potential and an entropic term proportional to the radius of the shell. The rate constants of the reactions at the surface of the excited molecule, k_{PT} and k_r, are typical for the pyranine and the specific properties of the solvent. The analysis is based on reconstruction of the observed signal through numerical integration of the Debye−Smoluchowski equation with a set of adjustable parameters, as listed in Table 1.

The rate constants that reconstruct the signal of the pyranine dissolved in water are given in Table 1, row 1. These values are consistent with numerous independent measurement of pyranine in water. The signals simulated by these parameters are superpositioned over the corresponding experimental traces, and the fitting is sufficient not to deviate out of the noise level of the recording.

The signals measured for the pyranine−γ-CD complex differ from those measured in water by two independent factors. The first one is the need for different values assigned to k_{PT} and k_r. The dissociation rate constant, k_{PT}, is smaller by a factor of 2 from that measured in water, while the recombination step is twice as fast. Altogether, these events render the ROH* state to be much more dominant during the dynamics. The other factor that had to be incorporated into the simulation of the pyranine−γ-CD complex was the presence of a proton scavenger[52] (Table 1, column 8). This reaction had to be added in order to gain the precise curvature of the fluorescence decay. The rate constant of the reaction with the scavenger was determined to be $k \sim 8.5 \times 10^7$ M^{-1} s^{-1}. By assuming that the scavenger reacts with the released proton in a diffusion-controlled reaction, $k \sim 5 \times 10^{10}$ M^{-1} s^{-1}, its apparent concentration, is ~1.5 mM. Such a high concentration for unaccounted scavenger cannot be attributed to unknown contaminant. What is more, a pH titration of the solution did not reveal the presence of any appreciable buffer capacity. Thus, we have to conclude that the scavenger present in the system is only a temporary proton binding site and not a persistent acceptor, a feature never previously observed.

It is of interest to point out that the values of the kinetic isotope effect, calculated for the proton dissociation and the recombination reaction, are in the order of 1.5−3.3. These values are within the range determined before, indicating that the mechanism is basically a normal diffusion with minimal contribution of tunneling or concerted proton transfer reactions.

Long-Time Fluorescence Decay Dynamics. According to the geminate recombination model, the long-time asymptotic decay of the ROH* emission is given as a power law of time, depending on the dimensionality of the diffusion space (eq 1). For a three dimension, the decay of ROH*(t) × exp(t/τ_f) follows a $t^{-3/2}$ power law. Figure 3 shows the ROH* decay of pyranine in aqueous solution and in the inclusion complex with γ-CD. While the data for pyranine in bulk water follows a power law of $t^{-3/2}$, the cyclodextrin complex data deviates from that power law.

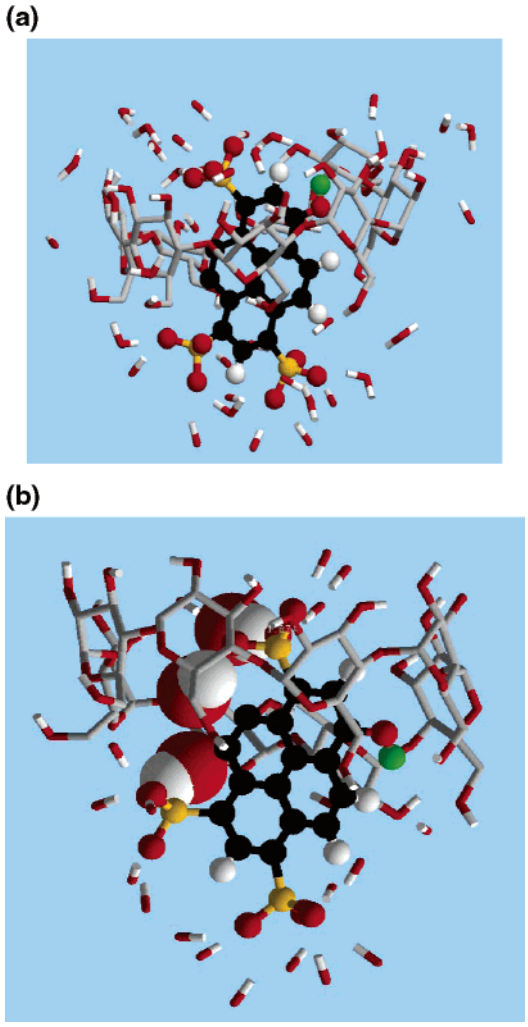

Figure 4. (a) Snapshots of ROH in γ-CD where the hydroxyl moiety is facing the 16 OH rim of γ-CD. (b) The less frequent configuration of the pyranine in the γ-CD torus where the hydroxyl moiety of pyranine is close to the 8 OH rim. Please note in this configuration a hydrogen-bonded string of three water molecules (depicted in their van der Waals radii) is formed.

The deviation from the power law decay, together with the appearance of the unaccounted scavenger, indicates that the geometry of the reaction space should be investigated at atomic resolution.

Solution Structure of the Pyranine−γ-CD Complex. The pyranine−γ-CD complex was simulated, with explicit water and Na^+ ions, to maintain electroneutrality. The complex was first subjected to energy minimization followed by a 6 ns simulation. As a control, we ran similar simulations of either the free γ-CD or the HPTS in water. Both structures were stable. The free pyranine was very rigid with a root-mean-square deviation (rmsd) of ~0.1 nm. The γ-CD was more flexible, exhibiting some "breathing" motion where the ring is flexing, having an rmsd value of ~0.3 nm. The complex between the two molecules was more rigid than the free γ-CD, having an rmsd of 0.25 nm (for the whole complex) and 0.2 nm for the γ-CD in the complex.

The most abundant orientation of the ROH is represented by the snapshot, appearing in Figure 4a, where for clarity the pyranine is colored in black and the hydrogen atom of its hydroxyl moiety is colored green. In this configuration, the hydroxyl is close to the 16 OH rim of the γ-CD. Examination of the water molecule in the vicinity of the complex reveals

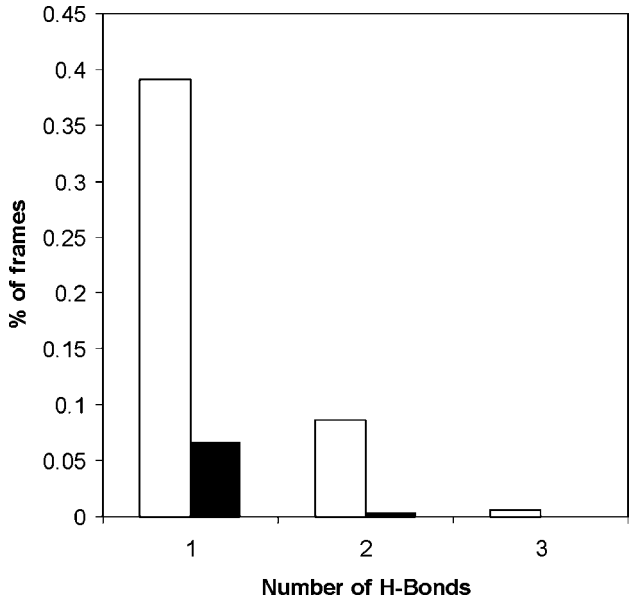

Figure 5. A histogram relating the propensity of the pyranine to form a hydrogen bond with few water molecules. The open columns relate to free pyranine in water, while the filled columns are for a pyranine molecule forming an inclusion complex with γ-CD.

that the γ-CD's hydroxyls and the sulfono moieties of the pyranine were well solvated, establishing a hydrogen bond with the water. However, the OH moiety of the ROH is somewhat withdrawn below the edge of the larger rim and is less available to form a hydrogen bond with the water (see also Figure 5). During the rattle of the pyranine in the γ-CD structure, it sometimes assumed another configuration, where the hydroxyl of the pyranine was even more secluded from the bulk (Figure 4b). In this location, the OH residue was close to the 8OH rim but hardly able to form a hydrogen bond with bulk water. In this configuration, where the pyranine structure is somewhat out of the polysugar torus, the inner free space, not occupied by the pyranine, can accommodate a string of three hydrogen-bonded water molecules, connecting the two sulfono moieties of the dye (Figure 4b). The lifetime of this configuration is less than 1 ns, which is significantly shorter than the lifetime of the excited pyranine molecule. Thus, the two configurations of the complex are well equilibrated and cannot be regarded as isolated structures each having its own dissociation dynamics.

Comparison between the two configurations, where that of Figure 4a appears to dominate by a ratio of ~9:1, indicates that when the dye is well embedded in the torus, there is no space for a water molecule. When the dye is partially removed from the inner space of the torus, water molecules can penetrate, forming a connecting structure between the sulfono moieties. Thus, the notion that hydronium ions can be trapped inside the γ-CD structure and serve as a donor for RO^{-}* can be considered as a low probability event, not sufficient to account for the 3-fold enhancement of the reprotonation of the RO^{-}*.

The insertion of the pyranine into the γ-CD frame reduces the number of the hydrogen bonds that can be formed with water. The free ROH has an average of 25 hydrogen bonds with the water, using both the sulfono moieties and the hydroxyl, with an average lifetime of 6.36 ps. The solvation of the ROH in the complex is somewhat reduced; only 21 hydrogen bonds (averaged) are formed with a longer lifetime of 8.36 ps. The two molecules do form hydrogen bonds between themselves, using the sulfono residues of the pyranine and the many hydroxyls of the γ-CD. However, maybe due to the rattling motion, the average number of hydrogen bonds that the pyranine

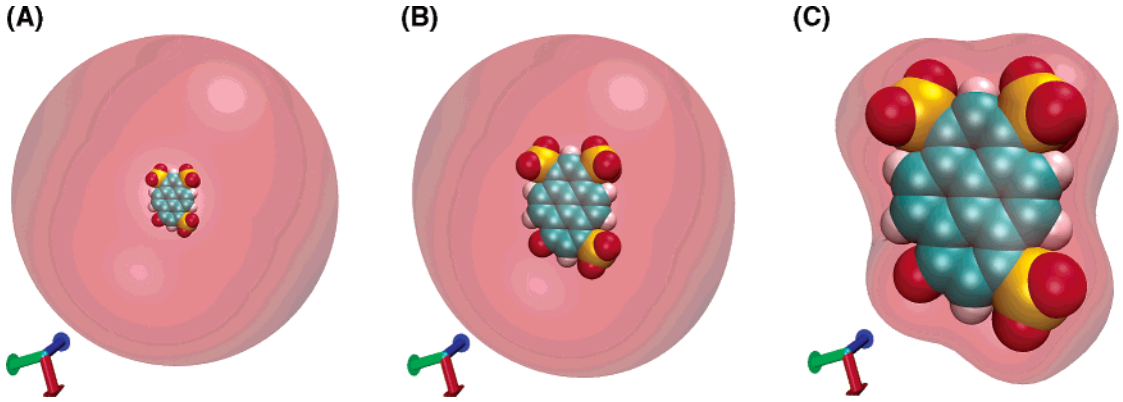

Figure 6. Visualization of the Coulomb cage around the free pyranine anion as calculated for an ionic strength of 120 μM. Frames A, B, and C draw the surface of the 1, 2, and 4.5 k_BT/electron boundary.

has with the γ-CD is less than 1 with a lifetime shorter than 2ps. These hydrogen bonds are similar in lifetime with the hydrogen bond (average 9.5 bonds, both for the free γ-CD and the complex) that the γ-CD forms with the bulk water.

Of the many hydrogen bonds that pyranine can form with water, the solvation of the hydroxyl is the most crucial for the photodissociation reaction. Inspection of the frequency of hydrogen bonds formed by the hydroxyl moiety, either of the free pyranine or in the inclusion complex, reveals a major decrement in the hydrogen-bond probability. During the 6000 ps simulation time of the free pyranine in bulk water, we recorded a single hydrogen bond, between the OH moiety of the dye with the water, in 38% of the snapshots and two hydrogen bonds in ~8% snapshots (Figure 5, open columns). In its γ-CD complex, the ability of the pyranine's hydroxyl to form a hydrogen bond with the water is drastically reduced. Only 6% of the snapshots revealed one hydrogen bond with the water and the fraction of two simultaneous hydrogen bonds was less than 1% (Figure 5, solid columns). This can be the explanation as to why the probability of proton dissociation (expressed by k_{PT}) had dropped in the γ-CD inclusion complex.

It must be clarified that the molecular dynamics simulations were carried out with the ground state of the pyranine, which exhibits a different charge distribution than the excited state. However, we can assume that the values derived by the comparison between the free and bound states of the pyranine can be used as an approximation for the effect of the polysugar torus on the excited state of the pyranine. Indeed, the reduced value of k_{PT}, as directly recorded from the experimental data, is well corroborated by the simulations of the ground state molecule. We can deduce from the simulations that the ROH* in the γ-CD should be considered as an assembly of nonidentical states, which differ in their level of solvation and exposure to the bulk. Yet, the whole population is characterized by a reduced accessibility to the solvent, which accounts for the modulation of the proton transfer reactions taking place from the hydroxyl residue to the solvent.

Electrostatic Potential of Pyranine Anion in Water. The rate constant for protonation of an anion, as given by the time-independent diffusion-controlled reaction rate constant, refers to the rate at which the proton crosses the outer perimeter of the Coulomb cage, set at 1 k_BT/e. Once the proton is inside the cage, the local electrostatic potential steers it toward the charged moieties at a time frame much shorter than the encounter time. In the present study, the proton is generated inside the cage so that the dynamics are controlled by the internal gradient of the potential, a term hardly detected by monitoring of diffusion-controlled reactions.

The dynamics of proton transfer within the Coulomb cage had been studied by Huppert et al.[53] who were able to resolve the excited state proton transfer reaction of 2-naphthol-3,6-disulfunate dynamics. The excited state proton transfer dynamics consist of two pathways, the dissociation of the proton into an ion pair and, in parallel, a proton transfer from the hydroxyl moiety reaction to the nearby SO_3^- moiety at position 3, which was linked by a single water molecule to the donor OH. Due to the high proximity, the reaction did not let the proton probe a major fraction of the intra-Coulomb cage space.

Figure 6 depicts the shape of the electrostatic potential that surrounds the pyranine anion ground state, showing the isopotential surfaces set as 1, 2, and 4.5 k_BT/e. Obviously, at the 1 k_BT/e level, the Coulomb cage is almost spherical, not revealing the geometry of the charges within the sphere. At the 2 k_BT/e level, the shape of the potential surface is still close to a sphere, and only at the 4.5 k_BT/e level, the isopotential surface follows the shape of the molecule. However, the isopotential surfaces are, in all cases, continuous. A free proton located within the Coulomb cage will propagate down the electrostatic gradient toward one of the negative charges or will move in an equipotential trajectory from the vicinity of one negative site toward another. This equipotential motion is responsible for the efficient funneling of the proton toward the O^- residues in the RO^{-}* anion.

The calculated electrostatic potentials around the pyranine−γ-CD complex are presented in Figure 7. The insertion of the pyranine in the torroid has a major effect on the electrostatic potential that surrounds the pyranine anion. At vanishing ionic strength, the 1 k_BT/e surface expands far into the bulk, well beyond the atoms of the γ-CD molecule, and the shape of the Coulomb cage is practically spherical, resembling that of the free pyranine. However, at higher potentials (2 and 4.5 k_BT/e), and unlike the case calculated for the free pyranine, the continuity of the isopotential surfaces is lost. The γ-CD structure forms a "belt" around the pyranine, splitting the potential field into two sections. The upper one in the figure engulfs the two sulfono residues, while the bottom one surrounds the oxyanion and the third sulfono group. Thus, for the pyranine−γ-CD complex, the connectivity of the two lobes is less efficient than in the case of the free pyranine.

Temporary trapping of a proton by the sulfonate lobe of the pyranine−γ-CD complex can explain the modulate relaxation dynamics we had previously observed. A precise calculation of the proton delay by the sulfonate lobe is, at present, too complex to execute. The reaction should be simulated with explicit water molecules and with full attention to the quantum-mechanical nature of the diffusion of proton in water. However,

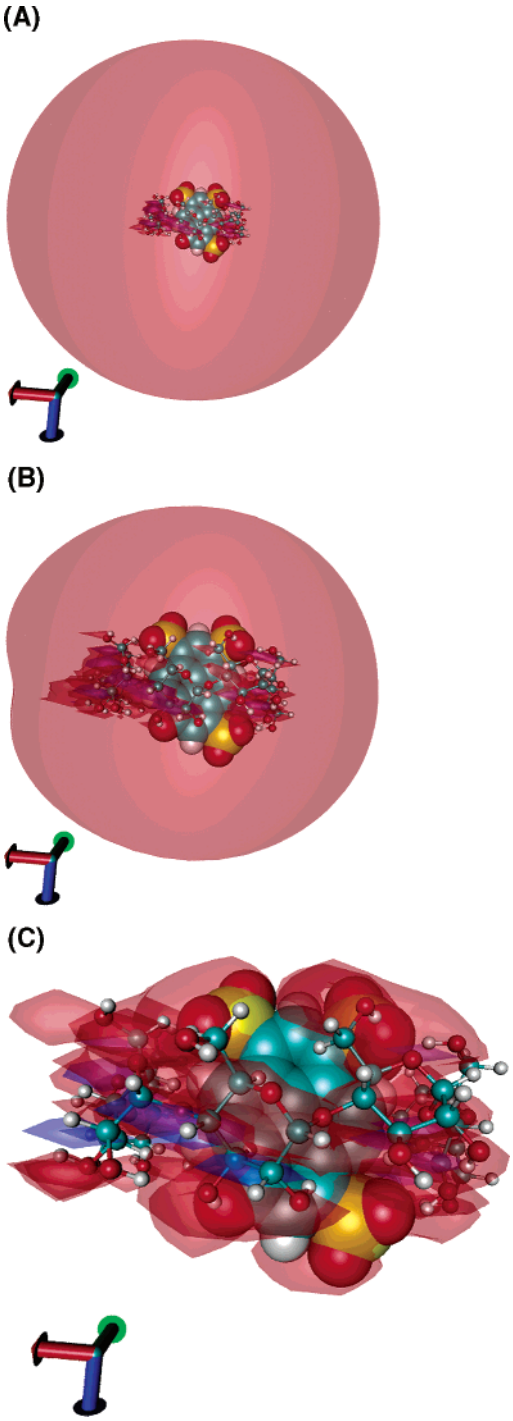

Figure 7. Visualization of the Coulomb cage around the complex of the γ-CD with the pyranine anion, as calculated for an ionic strength of 120 μM. Frames A, B, and C draw the surface of the 1, 2, and 4.5 k_BT/electron boundary.

an approximating calculation was carried out through the geminate recombination formalism. Assuming that the sulfonate lobe (see Figure 7, frames B and C) is disconnected from the acceptor lobe by a schism, the passage of a proton trapped in the sulfonates' lobe toward the one containing the oxyanion will follow a trajectory that emerges from that lobe through the bulk. The estimated escape time of a proton, from the sulfonate lobe to the bulk, is ~3 ns. Repeated re-entries of the proton into the sulfonate lobe can produce the temporary proton delay system, as was identified by the geminate recombination analysis. On the basis of the electrostatic potential calculation, we identify the proton scavenger function detected in the

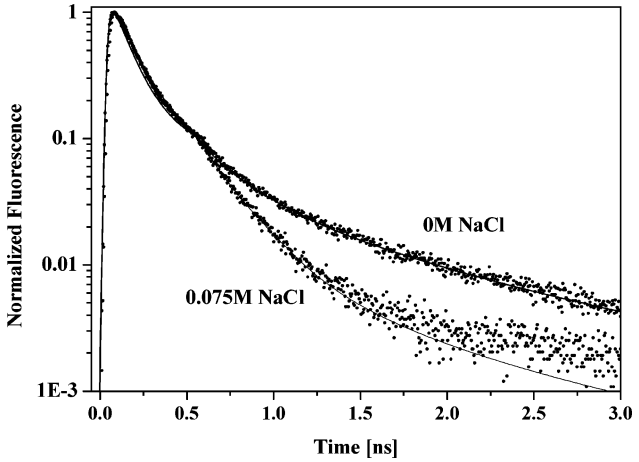

Figure 8. Semilog plot of the time-resolved emission and the computer fit using the geminate recombination model of the ROH* band of HPTS in water and in a 0.075 M NaCl solution.

presence of γ-CD as a reflection of the schism made between the two lobes, which render one acting as a competitor with respect to the other.

It should be explicitly stated that all of the above calculations were carried out for the ground state pyranine anion, while the kinetic measurements were with the first electronic singlet state, RO^{-}*. However, the electrostatic potential of the molecule, either in the free state or in complex with the cyclodextrin, is totally dominated by the $Z = -4$ charge. We argue that the modulation of the partial charges in the RO^{-}* state versus the RO^{-} will have only a minor effect on the shape of the Coulomb cage or the local potential inside the cage.

Interaction of the γ-CD Bound Pyranine with Bulk Reactants. The modulation of the reaction sphere of the pyranine by the torroid structure can affect the ability of solutes to react with the pyranine. This was tested by monitoring the fluorescence decay dynamics of the bound pyranine in the presence of acetate (acting as a proton scavenger), excess of free proton (acid effect), and, for control, in the presence of 75 mM NaCl screening electrolyte.

The decay dynamics as measured in the presence of 75 mM NaCl are given in Figure 8. At this concentration, the electrolyte concentration is too low to affect the activity of the water which determines the initial dissociation.[54] This can be seen by the superposition of the relaxation curves during the first ~700 ps. Beyond this time point, the proton released by the dissociation populates the immediate vicinity of the pyranine and the proton recombination reaction to form back the ROH* becomes noticeable, appearing as a slowdown in the fluorescence decay rate of ROH*. In the presence of the screening electrolyte, the Coulomb cage is diminished in size, enhancing the probability of the proton to escape out of the Coulomb cage, which diminishes the recombination process. This kinetic feature is typical for the presence of a scavenger, for which NaCl solution cannot be blamed. However, examination of the electrostatic potential surrounding the complex in 75 mM screening electrolyte reveals a sharper division between the two lobes of the Coulomb cage (not shown). Thus, the electrostatic potential calculation can provide an explanation for the effect of a screening electrolyte on the dynamics.

Addition of the acetate ion affects the dynamics, not only through the electrostatic screening effect but also through two reactions: one is with the free protons, and the other one is the deprotonation of the ROH* molecule upon encounter. Figure 9, which records the fluorescence decay dynamics of the

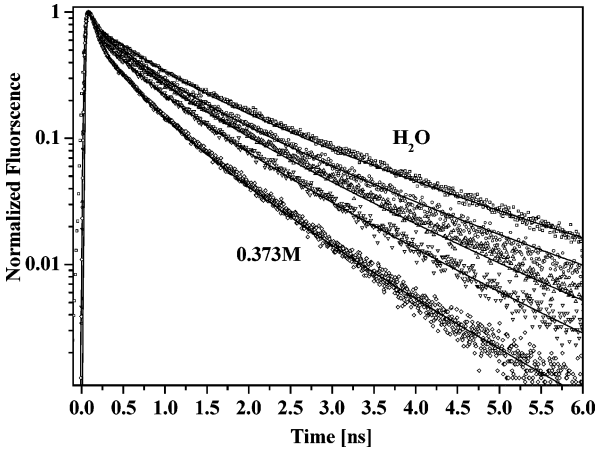

Figure 9. Time-resolved emission of the ROH* band of HPTS−γ-cyclodextrin in water with different concentrations of NaAc: 22, 63, 150, and 373 mM. Solid line, computer fit using the geminate recombination model.

TABLE 2: Kinetic Parameters for the Proton Transfer Reaction of HPTS−γ-CD in NaAc Solution

[NaAc] (M)	k_{PT}[a] (10^9 s^{-1})	k_r[a,b] (10^9 Å·s^{-1})	R_D (Å)	D_{H^+} (cm^2 s^{-1})	τ_{ROH} (ns)	τ_{RO^-} (ns)	k_{sc}[c] (s^{-1})
0.022	4.75	15.5	28	1×10^{-4}	5.4	5.4	1×10^9
0.063	5.0	15.5	28	1×10^{-4}	5.4	5.4	2.4×10^9
0.150	6.0	15.5	28	1×10^{-4}	5.4	5.4	3.2×10^9
0.373	7.0	11.5	28	1×10^{-4}	5.4	5.4	5×10^9

[a] k_{PT} and k_r are obtained from the fit of the experimental data by the reversible proton transfer model (see text). [b] The error in the determination of k_r is 50%; see text. [c] k_{sc}, pseudo-first-order proton scavenging rate constant; see text.

pyranine−γ-CD in the presence of increasing Na−acetate concentrations, depicts these features. The results of the analysis of the signals are listed in Table 2. At low concentration, the acetate functions as a screening electrolyte and the dynamics resemble that presented in Figure 6. The initial relaxation does not differ from that measured in water, but the depletion of the proton population renders the recombination to be slower, appearing as a steeper decay of the long-time behavior. At increasing acetate concentrations, the anion is sufficiently abundant to react with the free proton within the time frame of the observation, removing them from the system with subsequent depression of the recombination process. This reaction is given, as a pseudo-first-order rate constant, in the last column of Table 2. At an acetate concentration of ~0.4 M, the rate of encounter between the anion with the excited pyranine is sufficiently fast ($\tau \sim 0.5$ ns) so that direct deprotonation of the ROH* accelerates the deprotonation of the excited pyranine, appearing as a steeper decay of the most initial fluorescence. Indeed, at 150 and 373 mM acetate, the rate of the initial deprotonation (k_{PT}) of the pyranine is faster, and the rate constant, as given in the second column of Table 2, increases.

The Acid Effect. The excess proton effect on the protolytic cycle of photoacids was studied in the past.[55−61] In such an experiment, the pH of the aqueous solution is controlled by addition of small amounts of a strong acid like $HClO_4$. The ESPT cycle begins with transfer of a proton to the solvent. The proton recombination process is enhanced in solution containing excess homogeneous protons added to solution, as both bulk and geminate protons can recombine with RO^-*.[62]

With the ESPT in the presence of excess protons in bulk solution, the ROH time-resolved emission curve is composed of three components. The nearly exponential decay at short times

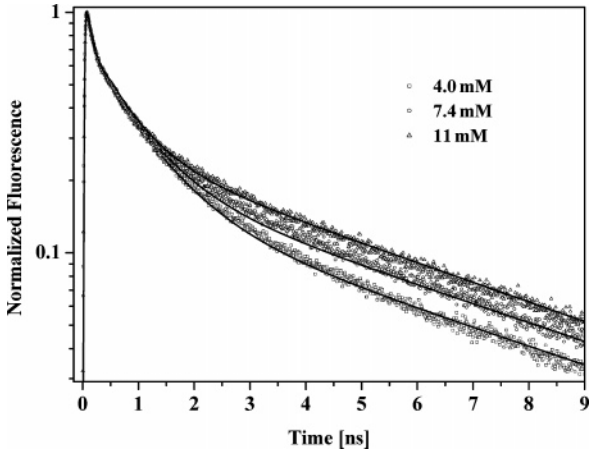

Figure 10. Time-resolved emission of the ROH* band of HPTS−γ-CD measurements along with a computer fit using the geminate recombination model (solid line), carried out with the pyranine−γ-CD complex, at increasing concentrations of a strong acid.

is mainly determined by a dissociation rate, which for HPTS is about (100 ps)$^{-1}$, and almost insensitive to both the geminate and excess protons' recombination process. The second component is a nonexponential long-time fluorescence tail which asymptotically assumes a power law of $t^{-3/2}$ in bulk solution. The amplitude of this component decreases with an increase of the mineral acid concentration. This component arises from the geminate proton recombination with RO^-* to form ROH*. The third component arises from the homogeneous chemical reaction between the excess proton and the RO^-*. It appears as an exponential tail in the ROH* time-resolved emission. The amplitude of the exponential tail increases with the acid concentration. The exponential decay time of this component depends on the excited state lifetime of both the ROH* and RO^-* forms of the photoacid.

The kinetics of the reversible dissociation and recombination of HPTS in the presence of excess homogeneous protons can be approximated by a simple model. To account for the homogeneous proton, we solve the DSE with spherical boundary conditions that partially account for the homogeneous protons. An outer reflecting sphere at a relatively long distance from the photoacid origin is placed at the calculations. When the geminate proton reaches the reflecting surface, it is reflected back to the diffusing volume. The effect is an increased recombination probability. In such a case, when the fluorescence of ROH* is multiplied by $\exp(t/\tau_f)$ the calculated values will not obey the $t^{-3/2}$ power law, the fusion in this case will exhibit a constant amplitude long-time tail. The outer sphere is placed at the average distance between the homogeneous protons. For 4 mM H^+, the distance is about 70 Å.

Figure 10 shows the time-resolved emission of the ROH band of HPTS in the inclusion complex with γ-CD in the presence of small concentrations of mineral acid ($HClO_4$) in solution, and a computer fit using approximate calculations along the lines previously described. As seen in the figure, the long-time fluorescence tail in the γ-CD complex increases with the acid concentration.

A difference is noticed between the experimental decay curves of HPTS in the bulk and in the inclusion complex with γ-CD. It refers to the relative amplitude of the exponential tail. In the case of HPTS in the complex with γ-CD, the amplitude is larger by about a factor of 3 than that in bulk water. This implies that excess protons in complexed HPTS are more effective to recombine with RO^-* than in the case of HPTS in bulk water.

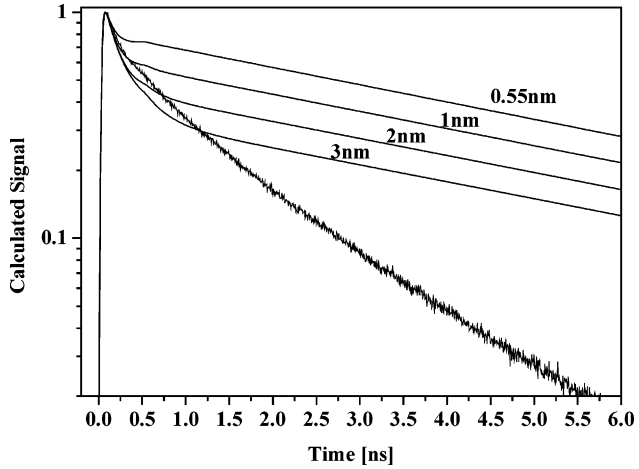

Figure 11. Simulations based on spherical cavities with reflection boundary conditions of the outer sphere. We displayed the calculated time-resolved emission of the protonated form, the ROH* of HPTS for several spheres whose radii vary from 3 to 0.5 nm along with a plot of the actual experimental data of HPTS ROH* in the inclusion complex with γ-CD.

This enhancement is attributed to the capacity of the hydroxyls on the rim to interact with the proton and, through a hydrogen-bond network, to share it with the oxyanion of RO^{-}*.

Simulation of the Protolytic Cycle of HPTS in a Small Confined Volume. Bahattacharyya and co-workers[27] explained the time-resolved emission data of HPTS in the inclusion complex with γ-CD as arising from the confinement of the just released proton within the polysugar torus. The inner diameter of the torroid cavity is quite small, about 9 Å, and its length is only 8 Å, of which most of it is taken by the pyranine molecule. The simulations reveal that, during most of the time, the pyranine molecule excludes any water from the inner space. Only in transient configurations, when the pyranine molecule partially retracts from the torus, a few (1−3) water molecules can temporarily penetrate into the inner space. In this subsection, we describe dynamics simulations, based on the GR model, of the ESPT process assuming that the released proton is indeed confined within the torus space; simulations were performed to check the possibility that the proton is detained inside the apolar inclusion volume, as suggested by Battacharyya and co-workers.[27] A good fit of the model calculation with the experimental results might indicate that, indeed, the protolytic cycle occurs within a confined volume.

The simulation of the proton dissociation from a photoacid in a confined spherical symmetric sphere, and its reversible geminate recombination cycle of a photoacid, is readily executed by the geminate recombination formalism. When the proton reaches the outer boundary sphere, it is reflected back to the confined volume surface. We assume that the proton motion within the confined volume is by diffusion, with a diffusion constant of bulk water of $D \sim 10^{-4}$ cm^2/s. Figure 11 shows such a simulation based on spherical cavities with reflection boundary conditions of the outer sphere. In the figure, we displayed the calculated time-resolved emission of the protonated form, the ROH of HPTS for several spheres whose radii vary from 3 to 0.55 nm along with a plot of the actual experimental data of ROH in the inclusion complex with γ-CD. As seen in the figure, the effect of a small reflecting spherical cavity with a radius of 0.55 nm (the inner diameter of the inclusion cavity) on the amplitude of the geminate recombination is much too large as compared to the experimental results. In the case that the diffusion constant is small, the amplitude of the long-time fluorescence tail of the ROH* increases. Basically, all of the simulations with spherical walls failed to fit the actual time-resolved emission curve of the ROH*.

Discussion

Small ions or medium size molecules that carry a large number of charges are readily approximated by a spheric Coulomb cage. Any reactant that ventures across the perimeter of the Coulomb cage reacts with the central target within a time frame shorter than the time needed for the encounter with the Coulomb cage. This approximation had been repeatedly tested by the proton pulse technique, and the accuracy of the approximation was persistently confirmed. A typical case for such a study is the rate of protonation of the ground state pyranine anion RO^{-}, which reacts with free proton with a rate constant of 1.6×10^{11} M^{-1} s^{-1}. The measured and calculated rate constants are essentially the same, demonstrating the validity of spheric symmetry as a model of the reaction space.[15,16]

The reactions inside the Coulomb cage are more complex than those in the entry phase. Within the cage, the pyranine exhibits four negative charges; only one of them is on the oxyanion. The reaction of the proton with the oxyanion leads to a detectable spectral shift, while an encounter with a SO_3^{-} residue has the same probability; however, the encounter is spectrally silent, making the protonation of the SO_3^{-} residue experimentally undetectable. The measured rate constant for the protonation of the RO^{-} has a value that specifies that all protons entering the Coulomb cage can react with no delay with the oxyanion site. This implies that the electrostatic potential within the Coulomb cage engulfs all negative charges, the SO_3^{-} residues and the O^{-}. Once the proton is inside the cage, it samples all locations in a smooth trajectory, moving from one site to another without mounting over a high range of barriers.

The reaction system investigated in the present study is fundamentally different from the previous studies, where the photoacid molecule was a free diffusing species. The insertion of the pyranine in the polysugar structure modulated the properties of the photoacid. The numerous hydroxyls located in the immediate vicinity of the dye interact with the solvent and reduce the ability of the innermost water molecule to function as a suitable acceptor with respect to the dissociating proton. In a similar way, the hydroxyls facilitate the probability of a bulk proton, by means of the existing hydrogen-bond system, to recombine with the oxyanion of the RO^{-}* species. The role of hydrogen-bonded water molecules had been previously implicated in proton transfer in biosystems. We suggest that the pyranine−γ-CD can be utilized as a model to study these reactions with sub-nanosecond resolution.

Another feature unique for the present system is the deformation of the Coulomb cage. The low dielectric constant torus perturbs the shape of the electrostatic field surrounding the pyranine anion and forms a schism between the sulfono domain and the oxyanion domain. As a result, the diffusion of the proton between the four negative centers, equally dispersed on the perimeter of the pyrene nucleus, is gravely disrupted. This distortion endows the system with kinetic features not found with the pure systems; a part of the molecule competes with the other for the free proton.

Finally, it must be recalled that, unlike the simple system composed of a photoacid in a solvent where we can assume that all molecules share the same environment, in the presence of the polysugar ligand, the system is better represented as a population of states, where the dye molecule experiences nonidentical conditions. The deviation from homogeneity

implies that straightforward application of the geminate recombination should also be assisted by molecular dynamics.

Bahattacharyya and co-workers[27] interpreted their observations by assumption of a model where the proton transfer process is confined by the γ-CD structure. Since inside the cyclodextrin cavity there is little space to allow a diffusive geminate ion pair recombination, another mechanism is required to account for the kinetic features recorded for the pyranine−γ-CD complex. We propose a different model that accounts for the large geminate recombination rate, which attributes the altered dynamics to the modulation of the ROH* environment by the γ-CD molecule. The 16 OH residues on the rim of the torus interact with the water in a manner that perturbs the interaction of the hydrogen bond between the hydroxyl of the ROH* and the solvent (see Figure 5 above), thus reducing the probability of proton transfer from the excited molecule to the water. In the same sense, the multitude of the OH residues, all properly forming a hydrogen-bond network with the solvent, function as a proton-collecting antenna that facilitates the probability of a bulk proton to react with the oxyanion of RO^-*. Thus, all kinetic features that discriminate between the free pyranine and its complex with γ-CD are fully attributed to the modulation of the pyranine's solvation shell by the polysugar.

Summary

Time-resolved and steady state emission techniques were used to study the photoprotolytic cycle of pyranine in the inclusion complex with γ-CD. We found that the proton transfer rate constant is reduced by a factor of 2 as compared with that in bulk water, while the geminate recombination rate constant is 3 times larger, in agreement with Bahattacharyya and coworkers.[27]

The results were interpreted by Bahattacharyya by a model assuming that the proton transfer process is confined by the γ-CD structure. Since inside the cyclodextrin cavity there is little scope of diffusion of the geminate ion pair, the main consequence of confinement seems to force the anion and the hydronium ion to stay in close proximity and thus the recombination process is enhanced.

We propose a different model accounting for the large geminate recombination rate. In general, the excited state cycle starts with a proton transfer to the solvent which is followed by a reversible proton geminate recombination to reform the ROH* in the excited state. The transport of the proton in the solution is by diffusion. The diffusion affects the recombination process, and as a consequence of the time-resolved fluorescence of the protonated form, ROH exhibits a nonexponential tail. Since the reaction is reversible, the ROH* can undergo a second protolytic cycle and so on. In the case of the inclusion complex of γ-CD and pyranine, the rate of the proton transfer step is decreased by about 50%. This fact seems to fit nicely to the structural scheme in which the OH group as well as the sulfonate groups of pyranine stick out from the cyclodextrin apolar cavity and both the OH and sulfonate groups are solvated by the water molecules surrounding the cyclodextrin structure. The proton transfer rate strongly depends on the nature of the solvent or the proton acceptor in general. The water serves as a very good proton acceptor as well as the ultimate solvent with a large dielectric constant ($\epsilon = 80$) to solvate the charged particles, the RO^- and the proton. As mentioned before, pyranine is incapable of transferring a proton in alcohols; thus, in an apolar cavity, it is unlikely that pyranine will transfer a proton within the excited state lifetime.

The second step in the protolytic cycle is the proton geminate recombination process. In the inclusion complex, the recombination is strongly enhanced compared with the recombination process of pyranine in bulk water. Simulations with reflective boundaries show that, in a small confined volume as the interior of γ-CD, the geminate recombination is overwhelmingly large, exceeding the experimental long-time tail intensity. This evaluation supports the model of proton transfer to the solvent rather than to the confined inner volume of γ-CD.

Molecular dynamics simulations and electrical potential calculations reveal that in the γ-CD inclusion complex the dynamics of the reversible proton dissociation is strongly affected by two mechanisms. On one hand, the low dielectric constant collar surrounding the pyranine introduces irregularities in the electrostatic field, introducing local energy barriers for a proton transfer within the boundary of the Coulomb cage. As a result, a fraction of the Coulomb cage functions as a temporary proton trap that delays the reaction of the proton with the oxyanion moiety of the excited pyranine. The other mechanism affecting the dynamics of the reaction is the modulation of the solvent properties by the multitude of OH moieties on the surface of γ-CD. The interaction of the water with the rims of the torroid structure renders the water to be a lesser proton acceptor, a poorer proton donor, properties which are detected both in the steady state and the kinetic features of the bound pyranine.

The present study reveals that the inner structure of the electrostatic potential within the boundary of the Coulomb cage can affect the observed dynamics. These effects cannot be fully quantitated by the geminate recombination formalism, yet the application of molecular modeling and molecular dynamics may provide an avenue for quantitative reconstruction of the intra-Coulomb-cage reactions.

Acknowledgment. We thank Prof. N. Agmon for his helpful and fruitful suggestions and discussions. This work was supported (DH) by grants from the Binational US-Israel Science Foundation, the James-Franck German-Israel Program in Laser-Matter Interaction and (MG) the United States-Israel Bi-National Science Foundation (Grant No. 2002129).

References and Notes

(1) Bell, R. P. *The Proton in Chemistry*, 2nd ed; Chapman and Hall: London, 1973.

(2) *Proton Transfer Reaction*; Caldin E. F., Gold V., Eds.; Chapman and Hall: London, 1975.

(3) (a) Weller, A. *Prog. React. Kinet.* **1961**, *1*, 189. (b) *Z. Phys. Chem. N. F.* **1958**, *17*, 224.

(4) (a) Eigen, M. *Angew. Chem., Int. Ed.* **1964**, *3*, 1. (b) Eigen M.; Kruse W.; Maass G.; De Maeyer, L. *Prog. React. Kinet.* **1964**, *2*, 285.

(5) Ireland, J. E.; Wyatt, P. A. *Adv. Phys. Org. Chem.* **1976**, *12*, 131.

(6) (a) Gutman, M.; Nachliel, E. *Biochim. Biophys. Acta* **1990**, *391*, 1015. (b) Pines, E.; Huppert, D. *J. Phys. Chem.* **1983**, *87*, 4471.

(7) Kosower, E. M.; Huppert, D. *Annu. Rev. Phys. Chem.* **1986**, *37*, 127.

(8) Tolbert, L. M.; Solntsev, K. M. *Acc. Chem. Res.* **2002**, *35*, 1.

(9) Rini, M.; Magnes, B. Z.; Pines, E.; Nibbering, T. J. *Science* **2003**, *301*, 349.

(10) Prayer, C.; Gustavsson, T.; Tarn-Thi, T. H. *Fast Elementary Processes in Chemical and Biological Systems*; 54th International Meeting of Physical Chemistry; AIP: New York, 1996; 333.

(11) Tran-Thi, T. H.; Gustavsson, T.; Prayer, C.; Pommeret, S.; Hynes, J. T. *Chem. Phys. Lett.* **2000**, *329*, 421

(12) Agmon, N. *J. Phys. Chem. A* **2005**, *109*, 13.

(13) Smith, K. K.; Huppert, D.; Gutman, M.; Kaufmann, K. *Chem. Phys. Lett.* **1979**, *64*, 22.

(14) Clark, J. H.; Shapiro, S. L.; Campillo, A. J.; Winn, K. J. *J. Am. Chem. Soc.* **1979**, *101*, 746.

(15) Pines, E.; Huppert, D. *J. Chem. Phys.* **1986**, *84*, 3576.

(16) Pines, E.; Huppert, D.; Agmon, N. *J. Chem. Phys.* **1988**, *88*, 5620.

(17) Gutman, M.; Huppert, D.; Nachliel, E. *Eur. J. Biochem.* **1982**, *21*, 637.

(18) Gutman, M.; Nachliel, E.; Huppert, D. *Eur. J. Biochem.* **1982**, 75−181.
(19) Nachliel, E.; Polak, N.; Huppert, D.; Gutman, M. *Biophys. J.* **2001**, *80*, 1498.
(20) Rochel, S.; Nachliel, E.; Huppert, D.; Gutman, M. *J. Membr. Biol.* **1990**, *118*, 225−232.
(21) Cohen, B.; Solntsev, K. M.; Huppert, D.; Nachliel, E.; Tsfadia, Y.; Gutman, M. *J. Am. Chem. Soc.* **2002**, *124*, 7539−7547.
(22) Agbaria, R. A.; Uzan, B.; Gill, D. *J. Phys. Chem.* **1989**, *93*, 3855.
(23) Lyashkevich, S. Yu.; Koz'menko, M. V.; Demyashkevich, A. B. *Khim. Fiz.* **1990**, *9* (10), 1324−1331.
(24) Koz'menko, M. V.; Lyashkevich, S. Yu.; Demyashkevich, A. B *Khim. Vys. Energ.* **1990**, *24* (6), 553−554.
(25) Koz'menko, M. V.; Lyashkevich, S. Yu.; Demyashkevich, A. B. *Khim. Vys. Energ.* **1990**, *24* (5), 451−455.
(26) Hansen, J. E.; Pines, E.; Fleming G. R. *J. Phys. Chem.* **1992**, *96*, 6904.
(27) Mondal, S. K.; Sahu, K.; Sen, P.; Roy, D.; Ghosh, S.; Bhattacharyya, K. *Chem. Phys. Lett.* **2005**, *412*, 228.
(28) Agmon, N.; Pines, E.; Huppert, D. *J. Chem. Phys.* **1988**, *88*, 5631.
(29) Rice, S. A. In *Diffusion-Limited Reactions.*; Bamford, C. H., Tipper, C. F. H., Compton, R. G., Eds.; Comprehensive Chemical Kinetics, Vol. 25; Elsevier: Amsterdam, The Netherlands, 1985.
(30) Agmon, N. *J. Chem. Phys.* **1984**, *81*, 2811.
(31) Agmon, N.; Goldberg, S. Y.; Huppert, D. *J. Mol. Liq.* **1995**, *64*, 161.
(32) Krissinel, E. B.; Agmon, N. *J. Comput. Chem.* **1996**, *17*, 1085.
(33) Lewis, G. N.; Doody, T. C. *J. Am. Chem. Soc.* **1933**, *55*, 3504.
(34) Haar, H. P.; Klein U. K. A.; Hfiner, F. W.; Hauster M. *Chem. Phys. Lett.* **1977**, *49*, 416.
(35) Berendsen, H. J. C., van der Spoel, D.; van Drunen, R. *Comput. Phys. Commun.* **1995**, *91*, 43−56.
(36) Lindahl, E.; Hess, B.; Van der Spoel, E. *J. Mol. Model.* **2001**, *7*, 306−317.
(37) van Der Spoel, D.; Lindahl, E.; Hess, B.; van Buuren, A. R.; Apol, E.; Meulenhoff, P. J.; Tieleman, D. P.; Sijbers, A. L. T. M.; Feenstra, A. K.; van Drunen, R.; Berendsen, H. J. C. *GROningen Machine for Molecular Simulations* 3.2.1. Groningen: 2004.
(38) van Gunsteren, W. F.; Billeter, S. R.; Eising, A. A.; Hunenberger, P. H.; Kruger, P.; Mark, A. E.; Scott, W. R. P.; Tironi, I. G. *Biomolecular Simulation: The GROMOS96 Manual and User Guide*; Vdf Hochschulverlag AG an der ETH Zurich: Zurich, Switzerland, 1996; pp 1−1024.
(39) Harata, K. *Bull. Chem. Soc. Jpn.* **1987**, *60*, 2763
(40) Schuttelkopf, A. W.; van Aalten, D. M. *Acta Crystallogr., Sect. D* **2004**, *60*, 1355−1363.
(41) Humphrey, W.; Dalke, A.; Schulten, K. *J. Mol. Graph.* **1996**, *14*, 33−38, 27−38.
(42) Berendsen, H. J. C.; Postma, J. P. M.; van Gunsteren, W. F.; Hermans, J. *Nature (London)* **1969**, *224*, 175−177.
(43) Hess, B.; Bekker, H.; Berendsen, H. J. C. *J. Comput. Chem.* **1997**, *18*, 1463−1472.
(44) Miyamoto, S.; Kollman, P. A. *J. Comput. Chem.* **1992**, *13*, 952−962.
(45) Berendsen, H. J. C.; Postma, J. P. M.; DiNola, A.; Haak, J. R. *J. Chem. Phys.* **1984**, *81*, 3684−3690.
(46) Essman, U.; Perela, L.; Berkowitz, M. L.; Darden, T.; Lee, H.; Pederse, L. G. *J. Chem. Phys.* **1995**, *103*, 8577−8592.
(47) Schmidt, M. W.; Baldridge, K. K.; Boatz, J. A.; Elbert, S. T.; Gordon, M. S.; Jensen, J. H.; Koseki, S.; Matsunaga, N.; Nguyen, K. A.; Su, S.; Windus, T. L.; Dupuis, M.; Montgomery. J. A. *J. Comput. Chem.* **1993**, *14*, 1347−1363.
(48) Baker, N. A.; Sept, D.; Joseph, S.; Holst, M. J.; McCammon, J. A. *Proc. Natl. Acad. Sci. U.S.A.* **2001**, *98*, 10037−10041.
(49) Solntsev, K. M.; Huppert, D.; Tolbert, L. M.; Agmon, N. *J. Am. Chem. Soc.* **1998**, *120* (31), 7981−7982.
(50) Solntsev, K. M.; Huppert, D.; Agmon, N. *J. Phys. Chem. A* **1998**, *102*, 9599−9606.
(51) Solntsev, K. M.; Huppert, D.; Agmon, N. *J. Phys. Chem.* **1999**, *103*, 6984−6997.
(52) Goldberg, S. Y.; Pines, E.; Huppert, D. *Chem. Phys. Lett.* **1992**, *192*, 77−81.
(53) Bart, E.; Huppert, D. *Chem. Phys. Lett.* **1992**, *195*, 37−44.
(54) Huppert, D.; Kolodney, E.; Gutman, M.; Nachliel, E. *J. Am. Chem. Soc.* **1982**, *104*, 6949.
(55) Loken, M. R.; Hayes, J. W.; Gohlke, J. R.; Brand, L. *Biochemistry* **1972**, *11*, 4779−4786.
(56) Ireland, J. F.; Wyatt, P. A. H. *Adv. Phys. Org. Chem.* **1976**, *12*, 131−221
(57) Laws, W. R.; Brand, L. *J. Phys. Chem.* **1979**, *83*, 795−802.
(58) Harris, C. M.; Selinger, B. K. *J. Phys. Chem.* **1980**, *84*, 891−898.
(59) Webb, S. P.; Philips, L. A.; Yeh, S. W.; Tolbert, L. M.; Clark, J. H. *J. Phys. Chem.* **1986**, *90*, 5154−5164.
(60) Krishnan, R.; Fillingim, T. G.; Lee, J.; Robinson, G. W. *J. Am. Chem. Soc.* **1990**, *112*, 1353−1357.
(61) Lima, J. C.; Abreu, I.; Brouillard, R.; Maçanita, A. L. *Chem. Phys. Lett.* **1998**, *298*, 189−195.
(62) Agmon, N. *J. Phys. Chem. A* **2005**, *109*, 13.